Shear alignment and orientational order of macroscopic rodlike grains

R. Stannarius*, S. Wegner*, B. Szabó† and T. Börzsönyi†

*Otto–von–Guericke–University, D–39106 Magdeburg, Germany
†Institute for Solid State Physics and Optics, HAS, Budapest, Hungary

Abstract. This contribution establishes a link between very different soft matter systems that exhibit orientational order. Granular matter research has been focused so far mainly on ensembles of spherical or irregularly shaped grains. Recently, several studies of anisometric particles have been reported, but still, many phenomena in such materials are little understood. Quantitative experiments are scarce. We report shear experiments with macroscopic shape-anisotropic particles [Börzsönyi et al., *Phys. Rev. Lett.*, **108**, 228302 (2012)] and discuss induced orientational order and alignment. Optical observations of the top layer are accompanied by X-ray computed tomography [Wegner et al., *Soft Matter*, in press (2012)], where positions and orientations of each individual grain in the bulk can be resolved. We establish quantitative relations between shear alignment and aspect ratio. The induced orientational order influences local packing and other macroscopic properties like the shear resistance. A comparison is drawn with molecular liquid crystals (LC). Many observations are qualitatively and even quantitatively comparable to the well-understood nematic phase of rodlike molecules, even though the types of interactions are completely different.

Keywords: granular flow, flow alignment, orientational order
PACS: 45.70.Mg, 83.50.Ax,61.30.Gd

INTRODUCTION

Shape-anisotropic particles are ubiquitous on all length scales in everyday life, from a molecular level to macroscopic grains (e.g. rice or beans). Industrial mass products of elongated shape include glass and plastic rods, screws, nails and wooden pegs. The interactions of individual particles can be very different, depending upon materials and sizes: van der Waals forces, electric dipolar interactions, capillary forces or hard-core steric repulsion, among others. Sometimes, hydrodynamic interactions with an interstitial fluid have to be taken into consideration. Several common phenomena are observed on all size levels. In particular, systems of all sizes can form local orientational order, and they can exhibit the tendency to align in shear flow.

The spontaneous formation of orientational order and alignment under shear flow are best investigated in molecular liquid crystals (LC). A mean field model (Maier–Saupe) describes orientational order in the nematic phase. The local director **n** is introduced to characterize the preferential direction of the mesogens. A well-established continuum model describes the viscous and elastic forces acting on the director (Leslie-Ericksen equations [1]). These equations are well confirmed by experiments. One typical phenomenon is the alignment of **n** with a small angle respective to the streamlines of a shear flow in the LC. This alignment can be quantitatively related to viscosity coefficients of the material. Recently, it has been demonstrated [2] that elongated macroscopic particles of cylinder or ellipsoid shape exhibit shear alignment in a very similar way, even on a quantitative level.

LC phases are formed not only by molecular building blocks. One finds them in suspensions of elongated nanocrystallites or nano-rods ([3]) or viruses ([4]). Bacteria [5, 6] or clay platelets in aqueous solutions [7, 8] form lyotropic LC mesophases. Shear-alignment has been observed in these systems, although often only qualitatively described (e.g. [9]).

Of special interest in connection with this study of granular rods are measurements of shear-induced birefringence in isotropic liquids [10]. This effect can be substantially large in the vicinity of the isotropic-nematic phase transition [11]. In these systems, shear flow has the combined effect of inducing orientational order and aligning the preferential orientation direction.

We study shear alignment of macroscopic cylindrical, sphero-cylindrical and ellipsoidal particles in the millimeter range. The positions and orientations of the individual particles under shear are detected by optical methods in the surface layer of the granulate, and by X-ray computed tomography (CT) in the volume. Under shear flow, we characterize the development of orientational order and shear alignment quantitatively, on the macroscopic ensemble level as well as on the individual particle level. We compare the observations to continuum models for nematics.

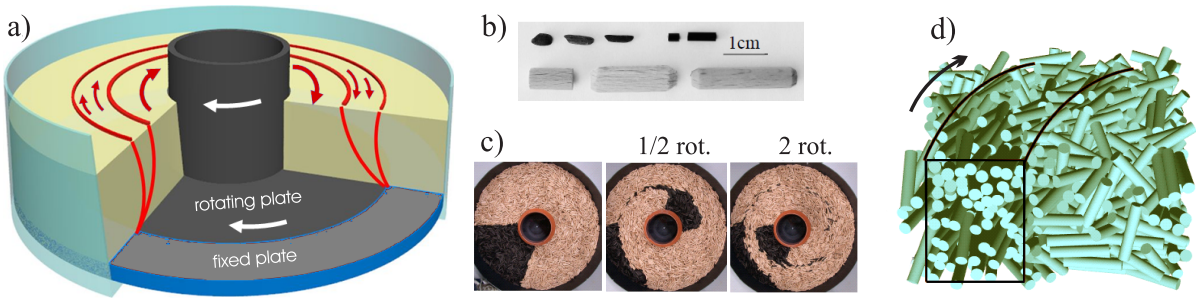

FIGURE 1. a) Split-bottom geometry: The inner cylinder, connected to a bottom disk with approximately half the radius of the container, can be rotated. The shear in the granulate is confined to a localized ring zone that extends from the bottom to the surface. b) Selection of investigated grains, rice grains and glass rods in the top row, and wooden pegs in the bottom row. c) Top views of the container, filled with wooden pegs. The outer diameter of the container is 60 cm. A 72° sector has been marked with brown pegs before shearing. The redistribution of the labeled pegs after 1/2 and 2 rotations visualizes the extension of the closed circular shear zone, centered around the outer edge of the rotatable bottom disk. d) Reconstruction of a typical rod arrangement in a section of the split-bottom cell. The positions and orientations of pegs with aspect ratio 5 were determined from an X-ray CT image. The solid lines indicate the approximate location of the shear zone.

EXPERIMENTAL SETUP

The experimental geometry is a cylindrical container with split bottom [12]. Figure 1a) shows the sketch of the setup, b) shows a selection of the investigated materials and c) shows top views of the cell during the experiments. We shear the granular material by rotating the inner part (central cylinder and bottom disk). The strain is localized in the so-called shear zone, which is indicated schematically in the figure. The radius of the shear zone is roughly equal to the radius of the bottom disk, which is large compared to the particle dimensions. In order to identify the shear zone geometry, a sector was marked with colored pegs (Fig. 1c). Outside the sheared ring zone, the marked pegs stay essentially unchanged, and in the center of the container they are displaced as a block with the rotating inner plate. Across the shear zone, they are distributed. Excavation of the granular bed allows us to identify the full geometry of this zone.

Experiments were performed with wooden pegs of three different aspect ratios $Q = L/D$: $Q = 5$ (length $L = 25$ mm, diameter $D = 5$ mm), $Q = 3.3$ ($L = 20$ mm, $D = 6$ mm), and $Q = 2$ ($L = 10$ mm, $D = 5$ mm). The pegs differ in minor shape details, some have a riffled surface, some have tapered ends. These properties have no significant influences on the shear alignment. Further experiments were done with cylindrical glass rods and with rice grains of axis ratios between 2 and 4.5.

Optical analysis

First, we analyze video sequences of the granulate surface, which yields the alignment in the top layer under continuous shear. For an easier identification, some of the particles are color labeled [2]. The shear profile at the surface is easily reconstructed from the images. The complete shear zone geometry can be retrieved by a destructive analysis, the excavation of the granular bed layer by layer. This optical technique can efficiently provide large amounts of data for statistics, it is simple and unexpensive. On the other hand, it is not easy to extract the three-dimensional (3D) orientation of the grains, and one has to confirm by other methods that the surface data are representative for the bulk.

X-ray computed tomography

A technique that can achieve this and provide the complete 3D arrangement of the grains is X-ray CT [13]. Tomographic data can be analyzed separately at the surface, in the bulk far from container boundaries, and near container walls. We employ a medical X-ray angiography machine (Siemens Artis zeego) at the INKA lab of Otto von Guericke University, Magdeburg. Spatial resolutions chosen were 2.03 pixel/mm and 1.48 pixel/mm. Sensitive volumes are 25.2 cm $\times$ 25.2 cm $\times$ 19 cm, and 34.8 cm $\times$ 34.8 cm $\times$ 24.4 cm, respectively. The first image is recorded after ten full rotations of the shear container, when initial transients are extinguished. During the data acquisition, the rotation is stopped. A series of subsequent scans is taken after further rotations of approximately 180° each. More than 130 measurements were performed for each grain type.

A typical result of an X-ray CT reconstructed image is shown in Fig. 1d). The approximate borders of the shear zone are indicated by solid lines. The particles in the recorded volume were detected by image processing software. The detected particles are represented by cylinders and visualized by a ray tracing algorithm.

TABLE 1. Bulk order and alignment angles of wooden pegs with different aspect ratios. Values for the surface region are given in parentheses.

Q	S	Δ	θ_a [deg]	φ_a [deg]
5.0	0.81 (0.76)	0.09 (0.02)	6.9 (9.1)	3.6 (4.3)
3.3	0.72 (0.68)	0.12 (0.05)	8.0 (10.8)	3.3 (3.1)
2.0	0.27 (0.20)	0.21 (0.19)	10.1 (13.4)	5.4 (3.2)

In the data evaluation, we distinguish between a surface region of ≈ 1 cm depth (two particle diameters) and the bulk in a 2 cm thick layer below this region. Orientation and alignment of these two regions are determined separately. In each series of experiments we collect between 10,000 and 20,000 particle positions per region. The X-ray CT data serve as evidence that the surface observations with the less expensive optical technique [2], are fairly representative for the bulk behavior.

Order and alignment data are derived numerically. We calculate the symmetric traceless order tensor $\boldsymbol{T}$:

$$T_{ij} = \frac{1}{2N} \sum_{n=1}^{N} \left(3\ell_i^{(n)} \ell_j^{(n)} - \delta_{ij} \right) \qquad (1)$$

from the particle orientations $\vec{\ell}^{(n)}$ (unit vectors along the axes of cylinders n), the sum is over all N detected particles. This tensor yields the primary order parameter S as its largest eigenvalue. A second, biaxial order parameter Δ is the difference of the two other eigenvalues of $\boldsymbol{T}$. The directions of its principal axes contain the alignment information. The shear alignment angle θ_a is the deviation of the principal axis corresponding to the eigenvalue S from the local tangent. A second angle φ_a, between the same axis and the shear plane, characterizes the mean deviation of the particles normal to flow and shear gradient. The particle symmetry ($\ell \equiv -\ell$) implies that orientations (θ_a, φ_a) and $(\theta_a + \pi, -\varphi_a)$ are equivalent, and we restrict the parameter range to $-\pi/2 \leq \theta_a < \pi/2$.

RESULTS

Order parameters and alignment angles for cylindrical pegs, obtained for X-ray CT, are listed in Table 1. These values show that the bulk and surface values (in parentheses) do not differ qualitatively, although certain systematic trends are found: bulk order parameters are systematically higher. The biaxiality is larger in the bulk. The bulk alignment angles θ_a are systematically smaller by about 25 %. The general trends with increasing aspect ratio are: larger order parameters, lower biaxiality, smaller alignment angles both in the bulk and at the surface. The flow alignment angle is visualized in Fig. 2. Simulation data by Török [2] confirm the general trend. The only difference between cylindrical and ellipsoidal particles is, that at comparable aspect ratios the latter ones have a slightly smaller alignment angle. Figure 3 visualizes the distribution of the orientation angles.

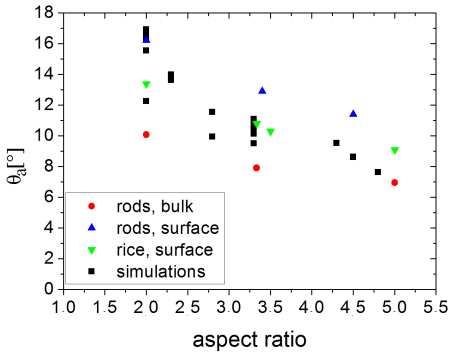

FIGURE 2. Alignment angle θ_a vs. aspect ratio Q. Simulation data (J. Török, [2]) are included for comparison.

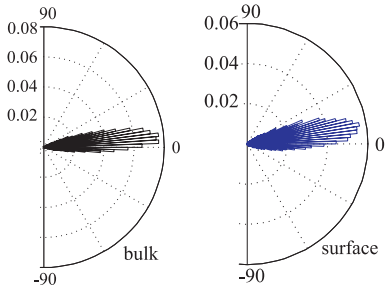

FIGURE 3. Distribution of the angles θ_a in the bulk (left) and in a 1 cm thick surface layer (right) for the pegs with aspect ratio 5, determined from X-ray CT.

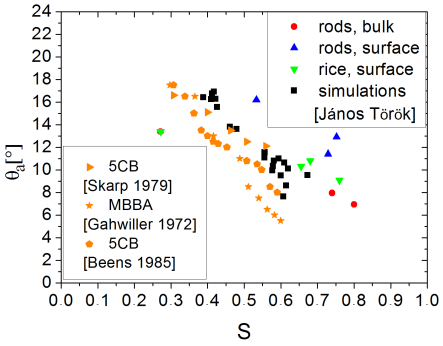

FIGURE 4. Relation between the alignment angle and the order parameter S. Data of thermotropic liquid crystals [14, 15, 16] are added for comparison.

The relations between the alignment angle and the induced order are shown in Fig. 4. In this graph, we added experimental values of two standard nematogens, MBBA and 5CB. It is remarkable that irrespective of fundamental differences of both systems, viz. type of interactions,

nature of the order parameter (thermodynamic vs. shear induced) and very different particle sizes, there is a clear similarity of the granular and molecular systems.

The alignment has consequences for the mechanical properties of the granulate. The shear-aligned samples show a reduced friction. This was obtained by torque measurements with the split-bottom cell [2].

Focusing on individual particle dynamics we find that in the asymptotic shear-aligned state particles rotate as dictated by the shear flow. The ensemble averaged angular velocity ω_{av} normalized by the shear rate $\dot{\gamma}$ as a function of the orientation θ is given in Fig. 5. Note that there is no fixed point in these curves, i.e. the particles are in effect rotating continuously, although with very different rates in different orientations to the flow. The continuity equation requires that the stationary distributions (Fig. 3) and the average reorientation rates are interrelated.

In addition to the structure and properties of the asymptotic shear-aligned state, we have studied the transients both from a non-oriented sample after initial preparation of the shear container and after reversal of the shear flow direction. It is interesting to analyze individual particle dynamics and to compare it to director dynamics in nematics. Shear flow reversal leads to a realignment where the majority of particles rotates with positive $\omega = d\theta/dt$ (see Fig. 5b), crossing the flow direction ('short path'), from $-\theta_{\mathrm{a}}$ to the new steady state θ_{a}. Only few particles perform a $2\theta_{\mathrm{a}} - 180^{\circ}$ turn with negative ω. In contrast, from a non-oriented state the majority of particles rotates with $\omega < 0$ towards θ_{a} ('long path').

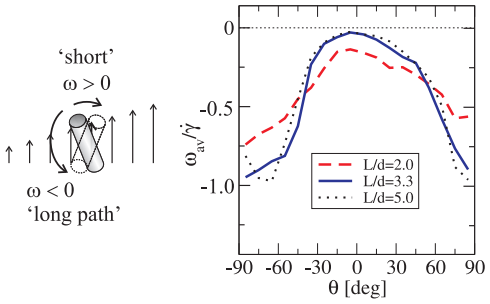

FIGURE 5. Average particle rotation ω_{av} in the asymptotic state in dependence upon their orientation, normalized by the shear rate. The drawing on the left sketches the reorientations.

SUMMARY

Qualitative and quantitative similarities have been found between the hydrodynamic effect of flow alignment in nematic LCs and the properties of elongated macroscopic grains. Orientational order is induced by shear, the preferential aligment forms an angle θ_{a} to the flow lines. This observation is related to a well known phenomenon in geology [17], so-called imbrication, where deposit material containing elongated grains helps e.g. to reconstruct flow pattern of past volcanic processes.

With increasing aspect ratio, the order parameter rises and the alignment angle decreases. Shear friction is reduced in the aligned samples. Individual particle dynamics have been analyzed. In the stationary state, the particles undergo a continuous rotation, where the average rotation rate is related to the particle orientation respective to the flow lines.

We thank G. Rose and T. Bien and the Inka Lab of Otto von Guericke University Magdeburg for the opportunity to use the X-ray CT facilities (funded by BMBF, reference No. 03IP710) and support. Financial funding from the DAAD-MÖB researcher exchange program No. 29480 is acknowledged.

REFERENCES

1. F. M. Leslie, *Quart. J. Mech. Appl. Math.*, 1966, **19**, 357.
2. T. Börzsönyi et al., *Phys. Rev. Lett.* **108** 228302 (2012).
3. e. g. W. H. Song, I. A. Kinloch, A. H. Windle, *Science*, 2003, **302**, 1363. A. Eremin, R. Stannarius, S. Klein, J. Heuer and R. M. Richardson, *Adv. Funct. Mater.*, 2011, **21**, 556. K. Kang, *Rev. Sci. Instrum.*, 2011, **82**, 053903.
4. e. g. C. Wetter, *Biologie in unserer Zeit*, 1985, **15**, 81. Z. Dogic and S. Fraden, *Phys. Rev. Lett.*, 1997, **78**, 2417. E. Grelet, M. P. Lettinga, M. Bier, R. van Roij and P. van der Schoot, *J. Phys.: Cond. Matter*, 2008, **20**, 494213.
5. D. Volfson, S. Cookson, J. Hasty and L. S. Tsimring, *PNAS*, 2008, **105**, 15346.
6. W. Mather, O. Mondragón-Palomino, T. Danino, J. Hasty and L. S. Tsimring, *Phys. Rev. Lett.*, 2010, **104**, 208101.
7. L. J. Michot, I. Bihannic, S. Maddi, C. Baravian, P. Levitz and P. Davidson, *Langmuir*, 2008, **24**, 3127.
8. D. van der Beek et al., *Phys. Rev. Lett.*, 2006, **97**, 087801.
9. F. C. Bawden, N. W. Pirie, J. D. Bernal and I. Fanhucken, *Nature*, 1936, **138**, 1051.
10. e. g. R. S. Wilkinson and G. B. Thurston, *Biopolymers*, 1976, **15**, 1555.R. E. Harrington, E. C. Uberbacher, and G. J. Bunick, *Nucl. Acids Res.*, 1982, **10**, 5695.C. Humbert and J. P. Decruppe, *Colloid Polym Sci*, 1998, **276** 160. *Eur. Phys. J. B*, 1998, **6**, 511. S. Lerouge, J. P. Decruppe, and C. Humbert, *Phys. Rev. Lett.*, 1998, **81**, 5457. C. Pujolle-Robic and L. Noirez, *Nature*, 2001, **409**, 167; *Phys. Rev. E*, 2003, **68**, 061706.
11. C. Bailey et al.,*Phys. Rev. Lett.*, 2009, **103** 237803.
12. J. A. Dijksman and M. van Hecke, *Soft Matter* **6** 2901 (2010).
13. S. Wegner, T. Börzsönyi, T. Bien, G. Rose, and R. Stannarius, *Soft Matter* **in press** (2012).
14. C. Gähwiller, *Phys. Rev. Lett.* **28**, 1554 (1972).
15. K. Skarp, S.T. Lagerwall, B. Stebler and D. McQueen, *Physica Scripta* **19**, 339 (1979).
16. W.W. Beens and W.H. de Jeu, *J. Chem. Phys.* **82**, 3841 (1985).
17. e. g. D.J.C. Laming, *J. Sediment. Petr.* 1966, **36** 940. D. Karátson, O. Sztanó and T. Telbisz, *J. Sediment. Res.*, 2002, **72**, 823..